

Synthesis, Characterization, and Photochromic Studies of Cyclometalated Iridium(III) Complexes Containing a Spirooxazine Moiety

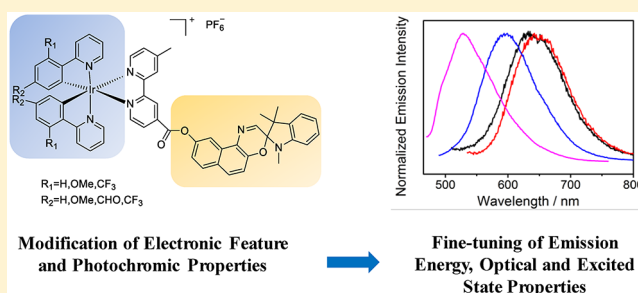
Jie Liu,^{†,‡} Alan Kwun-Wa Chan,[‡] Maggie Ng,[‡] Eugene Yau-Hin Hong,[‡] Nathan Man-Wai Wu,[‡] Lixin Wu,^{*,†,§} and Vivian Wing-Wah Yam^{*,†,‡,§}

[†]State Key Laboratory of Supramolecular Structure and Materials and College of Chemistry, Jilin University, Changchun 130012, PR China

[‡]Institute of Molecular Functional Materials (Areas of Excellence Scheme, University Grants Committee (Hong Kong) and Department of Chemistry, The University of Hong Kong, Pokfulam Road, Hong Kong SAR, PR China

Supporting Information

ABSTRACT: A series of cyclometalated iridium(III) complexes has been designed and synthesized, and their photophysical, photochromic, and electrochemical properties have been studied. The X-ray crystal structure of complex **2** has been determined. The emission properties of the complexes have been shown to be readily perturbed through the modification of the electronic properties of the phenylpyridine ligand. With different substituents at the phenylpyridine ligand of iridium(III) complexes of **1** (–H), **2** (–OMe), **3** (–CHO), and **4** (–CF₃), they can display intense ³MLCT [$d\pi(\text{Ir}) \rightarrow \pi^*(\text{diimine})$] luminescence from 530 to 640 nm to span across the green to orange region. The spectral assignment is also in agreement with the electrochemical studies and DFT calculations. In addition, the photochromic behavior can be easily modulated by varying the substituents on the C[^]N ligand without the need for tedious modification of the spirooxazine framework. By analyzing the kinetic profiles of backward bleaching reactions, less electron-rich iridium(III) complexes can stabilize the merocyanine form with a higher activation barrier. The studies have provided not only fundamental understanding on structure–property relationships that govern the versatile luminescence behavior of these Ir(III) complexes but also the guiding principles in the molecular design for the future developments of visible light-driven photoswitches.



INTRODUCTION

Due to the potential applications in the development of optical data storage, molecular switching and various other applications, the exploration of photochromic materials has attracted tremendous interests in many research areas.^{1–9} Photochromic spirooxazines are one of the most popular families among photochromic compounds due to their reversible chemical transformations and clean interconversion between two different molecular states simply triggered by light and heat.^{10,11} In general, spirooxazines undergo a photoinduced ring-opening reaction to form a merocyanine (MC) structure under UV light excitation, and most researches have focused on the organic system. It was only until 1998 that there has been a growing trend in the studies of integrating spirooxazine moiety as ligand into different metal centers to give interesting classes of metal complexes with novel and distinctive properties.^{12–21} In particular, one important strategy that has been demonstrated in these spirooxazine metal complex systems is the achievement of intramolecular photosensitization.^{13,17,20} One way to achieve photosensitization of the spirooxazine moiety is by intramolecular triplet energy transfer

from the visible light-absorbing metal-to-ligand charge transfer (MLCT) excited state using a less destructive and less harmful excitation source. For example, we have reported the photosensitization of spirooxazine moiety by ³MLCT excited state of rhenium(I) tricarbonyl diimine complex system.¹³ The strategy has also been adopted in other metal complex systems, for instance, Zn¹⁹ and Pt,²¹ as an important approach to fine-tune their photophysical and photochromic properties.

Cyclometalated iridium(III) complexes have been demonstrated to display intense phosphorescence at room temperature. They are widely explored in the field of organic light-emitting diodes (OLEDs) and molecular sensors as luminophores,^{22–29} while their utilizations in photochromic reaction or sensitization are relatively less explored. Moreover, the energy of the ³MLCT excited state of the Ir(III) complexes can be easily modulated by introducing different substituent groups on the cyclometalating C[^]N ligand to adjust the energy of the highest occupied molecular orbital (HOMO) as well as the

Received: May 27, 2019

Scheme 1. Synthetic Routes to Spirooxazine-Containing Bipyridine Ligand and Cyclometalated Iridium(III) Complexes

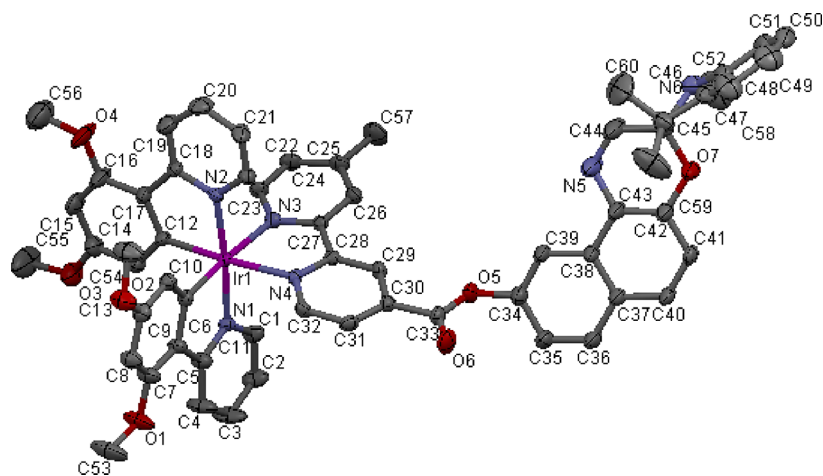
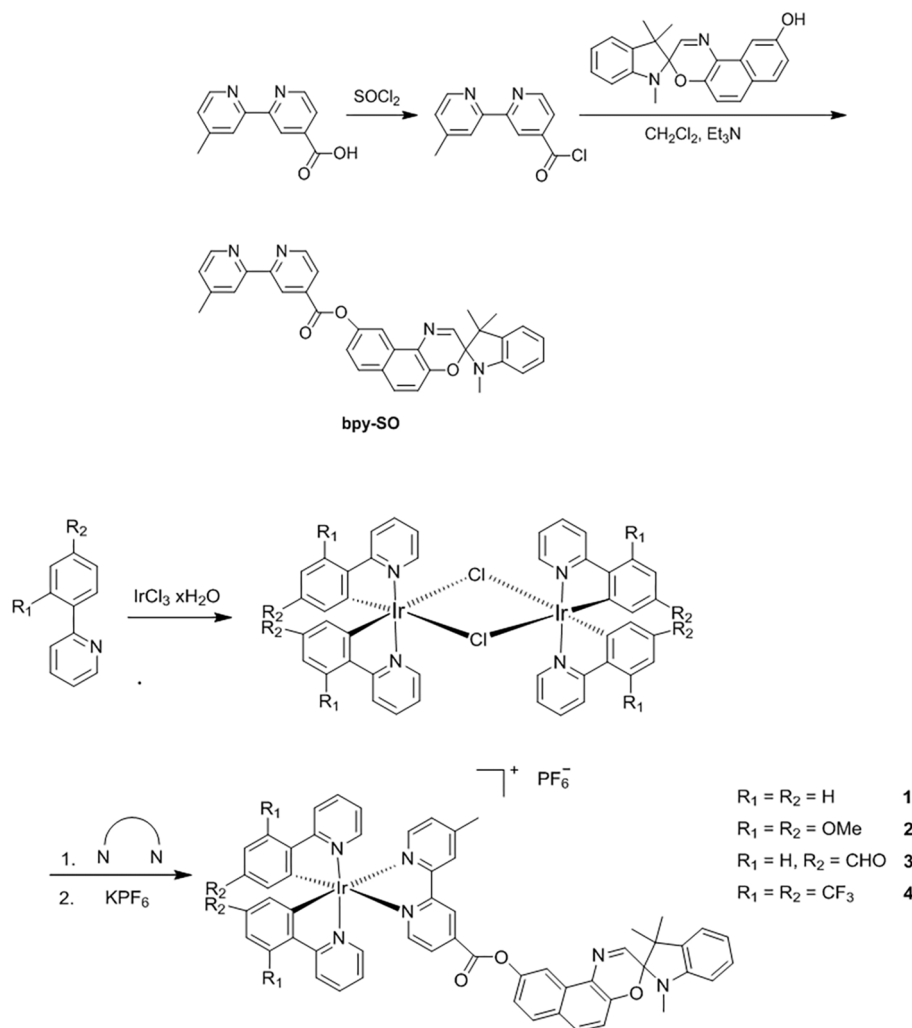


Figure 1. Structure of complex **2** with atomic numbering. Hydrogen atoms have been omitted for clarity. Thermal ellipsoids are shown at the 30% probability level.

overall optical bandgap. Therefore, it is envisaged that the combination of the rich excited state properties of Ir(III) complexes with the photochromic spirooxazine-containing ligand may provide attractive features for the development of multifunctional photoswitchable materials. Herein are described the design and synthesis of a series of spirooxazine-

containing cyclometalated Ir(III) complexes. Complexes **1–4** with the photochromic spirooxazine-containing diimine ligand, together with the phenylpyridine (ppy) ligands of different electronic properties, **1** (–H), **2** (–OMe), **3** (–CHO), and **4** (–CF₃) have been prepared to provide an in-depth investigation into fine-tuning their optical features (Scheme

1). The crystal structure and photophysical, photochromic, and electrochemical properties of these complexes have been investigated in detail to rationalize the molecular design strategy in coupling the tunable optical and excited state properties of the iridium(III) complexes for their application as photochromic materials.

RESULTS AND DISCUSSION

Synthesis. The synthetic routes of spirooxazine-containing bipyridine ligand (bpy-SO) and four iridium(III) complexes $[\text{Ir}(\text{C}^{\wedge}\text{N})_2(\text{bpy-SO})]^+\text{PF}_6^-$ (complexes 1–4) are shown in Scheme 1. The free ligand of bpy-SO was synthesized by modification of a literature method.¹⁷ The cyclometalated chloride-bridged Ir(III) dimers, $[\text{Ir}(\text{C}^{\wedge}\text{N})_2(\mu\text{-Cl})]_2$, were obtained by the Nonoyama reaction.³⁰ Substitution of $[\text{Ir}(\text{C}^{\wedge}\text{N})_2(\mu\text{-Cl})]_2$ with the diimine ligands in anhydrous dichloromethane at 50 °C, followed by metathesis with KPF_6 , afforded pure forms of complexes 1–4 after purification by column chromatography on silica gel and subsequent recrystallization from dichloromethane/hexane. The identities of iridium(III) complexes 1–4 have been confirmed by ¹H NMR spectroscopy, MALDI-TOF mass spectrometry, and satisfactory elemental analyses. Complex 2 has also been structurally characterized by X-ray crystallography.

X-ray Crystal Structure Determination. Single crystals of complex 2 have been obtained by slow diffusion of hexane into a concentrated dichloromethane solution of the complex. A perspective drawing of complex 2 is depicted in Figure 1, and the selected bond lengths and angles are summarized in Table 1. Complex 2 adopts a distorted octahedral geometry at

the iridium(III) atom, and the C–Ir–N and N–Ir–N bond angles are between 174.3 and 174.7°, deviating from the ideal 180° due to the steric demand exerted by the bite angles of the ppy-OMe and diimine ligands. The two ppy-OMe ligands are coordinated to the iridium(III) center in a cis configuration. The trans influence of the carbon donors renders slightly longer Ir–N bond lengths for the diimine ligand (2.139 and 2.151 Å) than that in the ppy-OMe ligand (2.038 and 2.042 Å). The bite angles of C–Ir–N in the ppy-OMe ligand (80.4 and 80.5°) are slightly larger than the N–Ir–N angle of the diimine ligand (76.3°). Similar observations have been reported in the related cyclometalated iridium(III) polypyridine systems, $[\text{Ir}(\text{C}^{\wedge}\text{N})_2(\text{N}^{\wedge}\text{N})]^+$.^{31–35} The bond length of the spiro C–O moiety in complex 2 is 1.461 Å, which is slightly longer than the common bond length of a C–O bond (1.43 Å) in other oxazine systems.^{36–39} This indicates that the spiro carbon–oxygen bond may be more readily cleaved when compared to the ordinary C–O bond, a phenomenon that is commonly found in the spirooxazine system.^{36–39} In addition, the interplanar angle between the indoline and naphthoxazine planes of 2 is 87.98°, which suggests an essentially orthogonal arrangement among these π -conjugated rings, possibly to minimize the steric repulsion between the spirooxazine system of neighboring molecules.^{19,37,38}

Photophysical Properties. The electronic absorption spectra of the free ligand, bpy-SO, in CH_2Cl_2 shows very intense intraligand (IL) π – π^* absorption bands of the bipyridine and indoline moieties at about 280 and 300 nm, as well as moderately intense IL π – π^* absorption of the naphthoxazine moiety observed at 318, 348, and 365 nm as reported in the literature.^{17,40} Complexes 1–4 in dichloromethane exhibit very intense absorptions at 280–360 nm and moderately intense bands at about 380–500 nm in their electronic absorption spectra (Figure S1). With reference to previous studies on iridium(III) bipyridine complexes and related spironaphthoxazine-containing transition metal complexes, the intense absorption bands at 280–360 nm are assigned to the IL π – π^* transitions of spirooxazine-containing bipyridine ligand and C[^]N ligands, whereas the relatively low-energy bands are assigned as a mixture of spin-allowed and spin-forbidden metal-to-ligand and ligand-to-ligand charge transfer (MLCT/LLCT) transitions.^{13,17,21,41–46} The photo-

Table 1. Selected Bond Lengths [Å] and Bond Angles [deg] with Estimated Standard Deviations (esds) in Parentheses for Complex 2

C(11)–Ir(1)	2.023(6)	Ir(1)–N(2)	2.042(5)
C(12)–Ir(1)	2.009(6)	Ir(1)–N(3)	2.151(5)
Ir(1)–N(1)	2.038(5)	Ir(1)–N(4)	2.139(5)
C(45)–O(7)	1.461(10)		
C(11)–Ir(1)–N(1)	80.5(2)	C(11)–Ir(1)–N(3)	174.4(2)
C(12)–Ir(1)–N(2)	80.4(2)	C(12)–Ir(1)–N(4)	174.3(2)
N(3)–Ir(1)–N(4)	76.25(19)	N(1)–Ir(1)–N(2)	174.72(19)

Table 2. Photophysical Data for the Complexes

compound	absorption λ_{max} [nm] (ϵ_{max} [$\text{dm}^3 \text{mol}^{-1} \text{cm}^{-1}$]) ^a	medium (T [K])	emission		
			λ_{em} [nm] (τ_0 [ns]) ^b	ϕ_{em}	k_r [s^{-1}] ^c
1	294 (45000), 368 (14120), 404 sh (9230), 494 (1600)	CH_2Cl_2 (298)	625 (44.8)	4.3×10^{-2}	9.59×10^5
1 (PMC) ^d		glass (77) ^e	540		
2	278 (51550), 294 sh (43740), 347 (29560), 390 sh (11370), 512 (1230)	CH_2Cl_2 (298)	640 (38.8)	3.5×10^{-2}	9.02×10^5
2 (PMC)		glass (77) ^e	550		
3	273 (67000), 292 (61850), 363 (20150), 384 sh (13020), 423 (6810), 478 (2880)	CH_2Cl_2 (298)	600 (4.4)	2.43×10^{-2}	5.54×10^6
3 (PMC)		glass (77) ^e	521, 563, 608		
4	322 (22930), 348 (16390), 420 sh (4650), 478 sh (1640)	CH_2Cl_2 (298)	530 (18.4)	6.19×10^{-2}	3.36×10^6
4 (PMC)		glass (77) ^e	489, 526, 560		
		glass (77) ^e	675		

^aIn dichloromethane at 298 K. ^bExcitation wavelength at ca. 420 nm. ^cEtOH–MeOH (4:1, v/v). ^dPMC: photomerocyanine form. ^eRadiative rate constant is calculated by $k_r = \Phi/\tau$, where Φ is the luminescence quantum yield and τ is the luminescence lifetime.

physical data for the ligand and the complexes are summarized in Table 2.

Upon excitation at $\lambda = 366$ nm, the free bpy-SO ligand exhibits two emission bands at 440 and 530 nm in CH_2Cl_2 at room temperature (Figure S2), attributed to the ligand-centered $\pi-\pi^*$ excited state.^{12,13,17} Excitation of complexes 1–4 in dichloromethane at $\lambda > 400$ nm at room temperature shows tunable luminescence properties (Figure 2). Intense

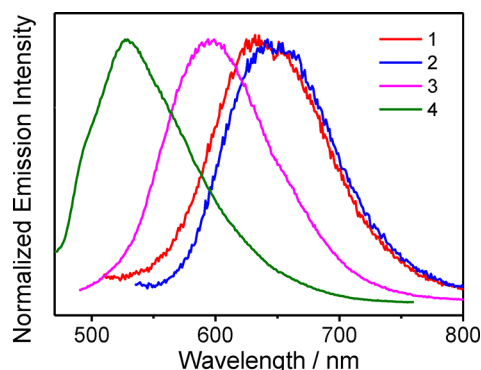


Figure 2. Normalized emission spectra of complexes 1–4 in degassed dichloromethane at room temperature.

structureless emission has been observed, and the emission energy maxima are between 530 and 640 nm, which are dependent on the electronic properties of the C^N ligands. These structureless emission bands are assigned to be originated from the ³MLCT [$d\pi(\text{Ir}) \rightarrow \pi^*(\text{diimine})$] excited state, probably mixed with some ³LC character for complexes 1–4. The increasing electron-deficiency of the aryl moiety on the C^N ligands from 2 (–OMe) to 1 (–H), to 3 (–CHO), and to 4 (–CF₃) would give a lower-lying $d\pi(\text{Ir})/\pi(\text{Ar})$ HOMO energy, leading to a gradual hypsochromic shift of the emission band, with emission energy in the order of 2 (640 nm) < 1 (625 nm) < 3 (600 nm) < 4 (530 nm), which is consistent with the ³MLCT/³LLCT(Ar → py) origin. This has also been supported by the TD-DFT calculations.

Complexes 1–4 also exhibit luminescence in EtOH–MeOH (4:1 v/v) glass from 489 to 608 nm at 77 K (Figure S3). The emissions are also tentatively assigned as ³MLCT phosphorescence, probably mixed with some ³LC character for 1–4. Upon excitation at 365 nm, the free ligand and complexes 1–4 in dry-ice–acetone baths at 195 K can also be transformed from the closed forms to the corresponding open forms with reduced thermal bleaching reaction rates. The open forms of complexes 1–4 and the free ligand show emission bands at 675–685 nm in EtOH–MeOH (4:1 v/v) glass at 77 K (Figure S4). The emission profiles and energies of the open merocyanine forms of the complexes and the free ligand are similar and insensitive to the change in the C^N ligands. Therefore, the emissions are assigned as ³LC phosphorescence of the merocyanine form of the spironaphthoxazine moiety.^{17,19,47}

Bleaching Reaction Kinetics. Complexes 1–4 have been found to display a drastic color change in degassed tetrahydrofuran solution upon excitation at 365 nm, attributed to the photochromic reaction. The mechanism of photochromic reaction of the spirooxazine is suggested to go through the photocleavage of the relatively weak spiro carbon–oxygen bond, resulting in the formation of the photomerocyanine form with an increased extent of π -conjugation at the photosta-

tionary state (PSS). However, the open form is thermally unstable and quickly undergoes bleaching reaction back to the closed form. The kinetics for the bleaching reactions of the merocyanine open forms of complexes 1–4, after excitation at 365 nm, have been investigated in tetrahydrofuran solution by UV–vis absorption spectroscopy at various temperatures. By monitoring the absorbance at 600 nm for complexes 1–4, the kinetic properties for the thermal backward bleaching reactions are measured and the activation parameters are determined using the Eyring and Arrhenius equations. The UV–vis spectral changes of the open forms of complexes 1–4 with time, along with the decay traces for the absorbance at 600 nm are shown in Figures S5–S12, and Figure S13 shows the difference in UV–vis spectra between the close form and open form in the Supporting Information. The Eyring and Arrhenius plots have also been constructed accordingly to obtain the thermodynamic activation parameters (Table 3). The positive values for

Table 3. Activation Parameters for the Bleaching Reaction of the Complexes in Tetrahydrofuran Solution

	ΔH^\ddagger (kJ mol ^{−1})	ΔS^\ddagger (J mol ^{−1} K ^{−1})	$\Delta G_{298\text{K}}^\ddagger$ (kJ mol ^{−1})	E_a (kJ mol ^{−1})
1	79.1 ± 1.59	19.86 ± 5.3	73.18 ± 3.17	81.59 ± 1.58
2	75.86 ± 1.09	11.36 ± 3.64	72.47 ± 2.17	78.35 ± 1.08
3	84.21 ± 1.32	35.39 ± 4.39	73.66 ± 2.63	86.71 ± 1.31
4	85.07 ± 1.73	37.81 ± 5.77	73.80 ± 3.45	87.56 ± 1.72

the activation enthalpies indicate that the bleaching reaction is a thermally activated process.^{17,19} The activation entropy of the complexes are determined to be in the range from +11.36 to +37.81 J mol^{−1}K^{−1}, which follow the same trend as their corresponding ΔH^\ddagger values. With the increase in electron deficiency of the C^N ligands (–OMe < –H < –CHO < –CF₃), the rates of the bleaching reaction decrease (2 > 1 > 3 > 4) at the same temperature with the ascending value of their ΔH^\ddagger and the free energy of activation $\Delta G_{298\text{K}}^\ddagger$ as well as the activation energy E_a . This may be due to the electron-deficient nature of the C^N ligands, which can stabilize the merocyanine form. Similar findings have also been reported on the stabilization of 6-nitro-merocyanine (6-nitro-BIPS) against thermal backward reaction to the spirooxazine form compared to the unsubstituted and more π -conjugated analogue,^{48,49} given the electron-deficient nature of the nitro-substituent which can inductively stabilize the dipolar resonance forms of merocyanine to increase the activation barrier for the thermal backward reaction.^{48,49} A careful investigation of the variation between ΔH^\ddagger and ΔS^\ddagger in complexes 1–4 has been performed and an isokinetic relationship has been observed (Figure 3). This shows a common bleaching reaction mechanism for the complexes. From the slope of the plot, an isokinetic temperature of 344 K for the bleaching reaction is obtained.

Besides, it is interesting to note that with the attachment of –CF₃ substituents to aryl ring of the C^N ligand, the ³MLCT excited energy of the current spirooxazine-containing cyclometalated iridium(III) system can be shifted to a higher energy of about 225 kJ mol^{−1} (530 nm), which is higher or comparable to the triplet excited state energies of spirooxazines (210–225 kJ mol^{−1}).¹⁷ Moderately intense MLCT absorption in the range of 400–500 nm in the visible region have also been observed in the current iridium(III) system. As a result, by further modifying their structure and electronic properties, it is possible to employ less destructive visible light to sensitize

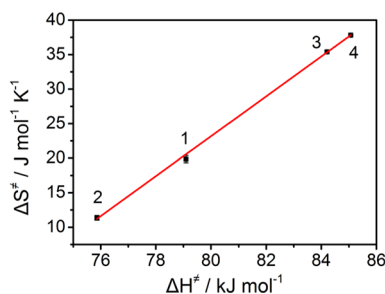


Figure 3. Plot of activation enthalpy against activation entropy for the bleaching reactions of the open forms of complexes 1–4.

the photochromic ring-opening reaction via the MLCT excited state. This further indicates the vital role in the structure–property correlation of the cyclometalated iridium(III) complexes and how this provides the tunability and functions as a unique class of photochromic materials. Therefore, with the appropriate molecular design strategy, it is possible to build versatile molecular materials with switchable and desirable functions.

Electrochemical Studies. The electrochemical properties of the cyclometalated iridium(III) diimine complexes are studied by cyclic voltammetry in acetonitrile (0.1 mol dm⁻³ Bu₄NPF₆). The electrochemical data are summarized in Table 4. Generally, complexes 1–4 show an irreversible

Table 4. Electrochemical Data for the Complexes in Acetonitrile Solution^a

compound	oxidation E_{pa} [V] vs SCE (ΔE_p [mV]) ^b	reduction $E_{1/2}$ [V] vs SCE (ΔE_p [mV]) ^c
1	[+1.11], +1.40 (80)	-0.91 (89), -1.47 (69)
2	[+1.11], +1.31 (81)	-0.92 (95), -1.49 (76)
3	[+1.11], +1.60 (70)	-0.88 (87), -1.46 (65)
4	[+1.12], +1.87 (84)	-0.88 (86), -1.40 (76)

^aUsing 0.1 mol dm⁻³ Bu₄NPF₆ at 298 K. Working electrode, glassy carbon; scan rate, 100 mV s⁻¹. ^b $\Delta E_p = (E_{pa} - E_{pc})$. ^c $E_{1/2} = (E_{pa} + E_{pc})/2$; E_{pa} and E_{pc} are peak anodic and peak cathodic potentials, respectively.

oxidation wave at ca. +1.11 V and a quasi-reversible oxidation couple at potentials between ca. +1.31 and +1.87 V versus SCE (Figures S14–S17). The first irreversible oxidative wave is assigned to the oxidation of the spirooxazine moiety, which is analogous to that observed for the related [Re(CO)₃(bpy-SO)Cl]¹⁷ and platinum(II) bipyridine complexes.²¹ With reference to the electrochemical studies on related classes of cyclometalated iridium(III) diimine complexes,^{50–56} the second quasi-reversible oxidation couples are assigned to metal-centered Ir(IV/III) oxidation process with significant contribution from the C[^]N ligands. The potential for the oxidation is found to be in the order 4 (+1.87 V) > 3 (+1.60 V) > 1 (+1.40 V) > 2 (+1.31 V), in line with the electron-deficient nature of the C[^]N ligands: -CF₃ > -CHO > -H > -OMe. The electron-deficient C[^]N ligand can stabilize the d π (Ir) orbital, rendering more positive potential required for the oxidation process.

In contrast, complexes 1–4 exhibit the first quasi-reversible reduction couples at ca. -0.88 to -0.92 V versus SCE, which is tentatively assigned to reduction of the diimine ligands (Figures S14–S17). The second quasi-reversible reduction couples at ca. -1.40 to -1.49 V versus SCE are tentatively

associated with the reduction of the C[^]N ligands, as they are commonly observed in related system.^{57–63} Even though the changes are small, the reduction potential can still be correlated to the electron-deficient nature of the C[^]N ligands, with 4 being most electron-deficient and having the least negative reduction potential (-1.40 V). The others follow the order 3 (-1.46 V) > 1 (-1.47 V) > 2 (-1.49 V), arising from the larger stabilization of the $\pi^*(C^{\wedge}N)$ orbital with the most electron-deficient C[^]N ligands. It is also noted that the trend of the HOMO–LUMO energies determined from the electrochemical studies is in accordance with their luminescence energies, suggesting the rational design strategy in fine-tuning the spectroscopic properties of the iridium(III) complexes by variation of their electronic features. This may provide the opportunity in coupling the spectroscopic properties to their functional applications.

Computational Study. To investigate the electronic structures and the nature of the absorption and emission origins of these iridium(III) complexes, density functional theory (DFT) and time-dependent DFT (TDDFT) calculations have been performed on complexes 1–4. Given in Figure S26 are the ground-state geometries of 1–4 optimized in dichloromethane with the hybrid B3LYP functional using the Coulomb-attenuating method (CAM-B3LYP),⁶⁴ which combines the hybrid qualities of B3LYP and the long-range correction. In 1–4, the Ir–C bonds are ca. 2.0 Å while the Ir–N bonds are ca. 2.1 Å, and the angles of the trans ligands at the metal center are ca. 173°, indicating that complexes 1–4 have similar structures. Moreover, the optimized structure of 2 is consistent with the experimental X-ray crystal structure shown in Figure 1, as their bond lengths and bond angles are close to each other. The simulated absorption spectra of 1–4 are shown in Figures S27–S30. The first 15 singlet–singlet transitions of 1–4 computed by the TDDFT/CPCM (CH₂Cl₂) method are summarized in Table S2, and selected molecular orbitals involved in the transitions are shown in Figures S31–S34. It should be noted that the singlet–triplet transitions have zero oscillator strengths as spin–orbit coupling is neglected in the TDDFT calculations. For the sake of the comparison of the low-energy singlet–triplet transitions in the experimental and simulated absorption spectra, the regions from 300 to 600 nm showing the singlet–triplet transitions with arbitrary oscillator strengths are included in the insets in Figures S27–S30. From Table S2 and Figures S31–S34, the S₀ → S₁ transitions of 1–4 have negligibly small oscillator strengths (0.001), so the S₀ → S₂ transition is considered. For 1, 3, and 4, the S₀ → S₂ transitions are attributed to the excitations from the d π orbital of the metal center with mixing of the π orbital on the C[^]N ligands to the π^* orbital on the C[^]N ligands. Therefore, their low-energy absorption bands can be assigned as ¹MLCT [$d\pi(\text{Ir}) \rightarrow \pi^*(C^{\wedge}N)$] transition. For 2, the S₀ → S₂ transition is attributed to the excitation from the d π orbital of the metal center with some mixing of the π orbital on the C[^]N ligands to the π^* orbital on the two pyridine moieties of the diimine ligand. As a result, the low-energy absorption band of 2 can be assigned as predominantly ¹MLCT [$d\pi(\text{Ir}) \rightarrow \pi^*(\text{diimine})$]/LLCT [$\pi(C^{\wedge}N) \rightarrow \pi^*(\text{diimine})$] transition. Due to the large spin–orbit coupling associated with the heavy Ir atom, it is possible for the spin-forbidden singlet-to-triplet MLCT transition computed at 430–480 nm to also have some contribution to the low-energy absorption band.

Given in Figure 4a is the orbital energy level diagram, which shows the energies of the frontier molecular orbitals of 1–4.

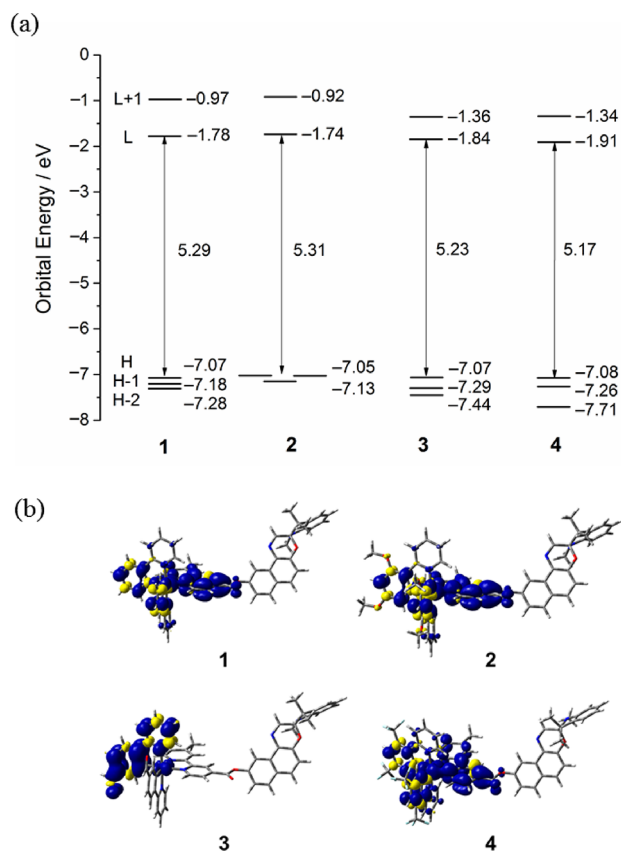


Figure 4. (a) Orbital energy level diagram of the frontier molecular orbitals (H = HOMO and L = LUMO) and (b) plots of spin density (isovalue = 0.002) of the T_1 states of 1–4 optimized at the CAM-B3LYP level.

Consistent with the results of the electrochemical studies, the HOMOs of 1–4 are of similar energies, which range from -7.08 to -7.05 eV. For all complexes except 2, the HOMOs are the π orbitals localized on the indoline moiety of the diimine ligand and, therefore, are less affected by the substituents on the two $C^{\wedge}N$ ligands. For 2, the HOMO is the $d\pi$ orbital on the metal center mixed with the π orbital on the $C^{\wedge}N$ ligands, which is degenerate with the HOMO–1, where the π orbital is localized on the indoline moiety of the diimine ligand. The LUMO of 2 (-1.74 eV) is less negative than that of 1 (-1.78 eV), whereas those of 3 (-1.84 eV) and 4 (-1.91 eV) are more negative than that of 1. Since the LUMOs of 1–4 are predominantly localized on the two pyridine moieties of the diimine ligand, the LUMO would be destabilized upon the introduction of the electron-donating $-OMe$ group to the $C^{\wedge}N$ ligands in 2 and stabilized upon the introduction of the electron-deficient $-CHO$ and $-CF_3$ groups to the $C^{\wedge}N$ ligands in 3 and 4. The above trends are consistent with the results in the electrochemical studies, in which the potentials of the irreversible oxidation wave of the four complexes are more or less the same. In comparison to 1, complexes 3 and 4 have less negative reduction potentials, and 2 has more negative reduction potential. As a result, 3 (5.23 eV) and 4 (5.17 eV) have a narrower HOMO–LUMO energy gap, while the energy gap of 2 (5.31 eV) is larger with respect to 1 (5.29 eV).

To further investigate the nature of the emissive states, geometry optimizations on the lowest-lying triplet excited state (T_1) of 1–4 have been performed with the unrestricted formalism, namely, UCAM-B3LYP/CPCM (CH_2Cl_2). Shown in Figure 4b are the plots of spin density of the T_1 states of 1–4. The spin density is mainly localized on the metal center and the $C^{\wedge}N$ ligands in all complexes and on the two pyridine moieties of the diimine ligand in 1, 2, and 4, supporting the 3MLCT [$d\pi(Ir) \rightarrow \pi^*(C^{\wedge}N$ or diimine)] character of the T_1 states of 1–4, with some mixing of 3LLCT [$\pi(C^{\wedge}N) \rightarrow \pi^*(diimine)$] character in 1, 2, and 4. The emission wavelengths of 1–4, which are approximated by the energy difference between the S_0 and T_1 states at their corresponding optimized geometries, are summarized in Table S3. The emission wavelength shows a red shift in energy upon going from 4 (472 nm) to 2 (479 nm), to 3 (484 nm), and to 1 (552 nm). In general, this trend is in fair agreement with that observed in the experiment, except that the emission energy of 2 is overestimated, as observed in other theoretical studies in which the CAM-B3LYP functional usually overestimates transition energies.^{65–67}

CONCLUSION

A new class of spironaphthoxazine-containing cyclometalated Ir(III) complexes has been designed, synthesized, and characterized. Their photophysical, photochromic, and electrochemical properties have been studied. Readily tunable luminescence colors and excited state properties can be achieved by rational ligand design with respect to their chemical intuition. It is interesting to note that the excited energy state can be gradually tuned across the visible spectrum with respect to the 3MLCT [$d\pi(Ir) \rightarrow \pi^*(diimine)$] excited state by a simple modification of the substituent at the $C^{\wedge}N$ ligand. The electrochemical data are also found to be in accordance with their luminescence bandgap energies. The nature of the absorption and emission origins of these iridium(III) complexes have also been confirmed by DFT and TDDFT calculations. More importantly, the photochromic behavior can be easily and complementarily modulated by changing the substituents on the $C^{\wedge}N$ ligand without the need for tedious modification of the spirooxazine framework. By analyzing the kinetic profiles of backward bleaching reactions, more electron-deficient iridium(III) complexes can stabilize the merocyanine open form with a higher activation barrier. Additionally, by further optimizing the molecular design, it is possible to employ less destructive visible light to drive the photochromic ring-opening reaction via the MLCT sensitization. This work may provide important value and guiding principle, especially in the structure–property correlation for the future developments of visible light-driven photoswitches, which is less destructive for potential applications of photoresponsive materials.

EXPERIMENTAL SECTION

Materials and Reagents. 4'-Methyl-2,2'-bipyridine-4-carboxylic acid,⁵⁷ 1,3,3-trimethyl-9'-hydroxy-spiroindolenaphthoxazine (SO),⁵⁸ 2-(2,4-bis-trifluoromethyl-phenyl)-pyridine,⁵⁹ and 2-(2,4-dimethoxy-phenyl)-pyridine⁶⁰ were synthesized as described previously. 1,3,3-Trimethyls-pirolindolenaphth-oxazine-9'-yl4'-methyl-2,2'-bipyridyl-4-carboxylate (bpy-SO) was synthesized by modification of a reported procedure.¹⁷ Dichloromethane was distilled over calcium hydride before use for synthesis. All other reagents were analytical-grade and were used as received.

Syntheses. [(ppy)₂Ir(μ-Cl)]₂ (Di-μ-chlorotetrakis[2-(2-pyridinyl-κN)phenyl-κC]di-iridium). IrCl₃·xH₂O (263 mg, 0.88 mmol) and 2-phenylpyridine (300 mg, 1.94 mmol) were dissolved in ethoxyethanol (15 mL) and water (5 mL). The mixture was refluxed under N₂ for 24 h. After cooling down to room temperature, the system was filtered and washed by ethanol. The product was isolated as a yellow solid. Yield: 262 mg, 56%. ¹H NMR (500 MHz, CDCl₃, 298 K, relative to Me₄Si): δ = 9.27 (d, J = 6.5 Hz, 4H), 7.89 (d, J = 7.8 Hz, 4H), 7.76 (t, J = 7.2 Hz, 4H), 7.51 (d, J = 7.8 Hz, 4H), 6.82–6.74 (m, 8H), 6.58 (t, J = 7.2 Hz, 4H), 5.95 (d, J = 6.5 Hz, 4H).

[(dOMeppy)₂Ir(μ-Cl)]₂ (Di-μ-chlorotetrakis[2-(2-pyridinyl-κN)-3,5-bis(methoxyl)phenyl-κC]di-iridium). The procedure was similar to that described for the synthesis of [(ppy)₂Ir(μ-Cl)]₂ except 2-(2,4-dimethoxy-phenyl)-pyridine (417 mg, 1.94 mmol) was used in place of 2-phenylpyridine. Yield: 317 mg, 55%. ¹H NMR (500 MHz, CDCl₃, 298 K, relative to Me₄Si): δ = 9.22 (d, J = 5.2 Hz, 4H), 8.58 (d, J = 9.8 Hz, 4H), 7.64 (dd, J = 9.8, 5.2 Hz, 4H), 6.63 (t, J = 5.2 Hz, 4H), 5.94 (d, J = 2.2 Hz, 4H), 5.10 (d, J = 2.2 Hz, 4H), 3.86 (s, 12H), 3.35 (s, 12H).

[(pba)₂Ir(μ-Cl)]₂ (Di-μ-chlorotetrakis[5-formyl-2-(2-pyridinyl-κN)-phenyl-κC]di-iridium). The procedure was similar to that described for the synthesis of [(ppy)₂Ir(μ-Cl)]₂ except 4-(2-pyridinyl)-benzaldehyde (355 mg, 1.94 mmol) was used in place of 2-phenylpyridine. Yield: 281 mg, 54%. ¹H NMR (500 MHz, CDCl₃, 298 K, relative to Me₄Si): δ = 9.52 (s, 4H), 9.27 (d, J = 5.8 Hz, 4H), 8.05 (d, J = 8.1 Hz, 4H), 7.93 (t, J = 7.8 Hz, 4H), 7.67 (d, J = 8.1 Hz, 4H), 7.30 (dd, J = 7.8, 1.4 Hz, 4H), 6.98 (t, J = 5.8 Hz, 4H), 6.36 (d, J = 1.4 Hz, 4H).

[(dCF₃ ppy)₂Ir(μ-Cl)]₂ (Di-μ-chlorotetrakis[2-(2-pyridinyl-κN)-3,5-bis(trifluoromethyl)-phenyl-κC]di-iridium). The procedure was similar to that described for the synthesis of [(ppy)₂Ir(μ-Cl)]₂ except 2-(2,4-bis-trifluoromethyl-phenyl)-pyridine (566 mg, 1.94 mmol) was used in place of 2-phenylpyridine. Yield: 400 mg, 56%. ¹H NMR (500 MHz, CDCl₃, 298 K, relative to Me₄Si): δ = 9.24 (d, J = 5.2 Hz, 4H), 8.47 (d, J = 8.2 Hz, 4H), 8.00 (t, J = 8.2 Hz, 4H), 7.49 (s, 4H), 7.04 (t, J = 6.5 Hz, 4H), 6.02 (s, 4H).

Complex 1. The complex was prepared by a modification of literature method used for the related Ir^{III} diimine complexes.^{61,62} [(ppy)₂Ir(μ-Cl)]₂ (246 mg, 0.23 mmol) and bpy-SO (270 mg, 0.5 mmol) were refluxed in degassed dichloromethane under nitrogen for 3 days. After cooling down to room temperature, KPF₆ (418 mg, 2.3 mmol) was added, and the mixture was stirred for 2 h. After removal of the solvent under reduced pressure, the residue was purified by column chromatography with dichloromethane-ethyl acetate (60:1 v/v) as eluent. Subsequent recrystallization of the product from dichloromethane/hexane afforded the pure product. Yield: 354 mg, 65%. ¹H NMR (500 MHz, CDCl₃, 298 K, relative to Me₄Si): δ = 9.13 (s, 1H), 8.39 (d, J = 9.4 Hz, 2H), 8.18 (d, J = 5.6 Hz, 1H), 8.07 (dd, J = 5.6, 1.2 Hz, 1H), 7.90 (d, J = 8.1 Hz, 2H), 7.80 (d, J = 5.6 Hz, 1H), 7.75 (dd, J = 15.0, 7.5 Hz, 2H), 7.69 (d, J = 8.9 Hz, 3H), 7.65 (d, J = 5.7 Hz, 1H), 7.57 (dd, J = 9.3, 5.2 Hz, 3H), 7.29 (dt, J = 8.8, 2.4 Hz, 1H), 7.22 (t, J = 7.7 Hz, 1H), 7.18 (s, 1H), 7.15 (t, J = 6.6 Hz, 1H), 7.10 (dd, J = 12.9, 6.8 Hz, 2H), 7.03 (td, J = 7.5, 2.4 Hz, 2H), 6.99 (d, J = 8.9 Hz, 1H), 6.91 (dt, J = 14.4, 7.1 Hz, 3H), 6.57 (d, J = 7.8 Hz, 1H), 6.32 (dd, J = 22.6, 7.4 Hz, 2H), 2.73 (d, J = 3.9 Hz, 3H), 2.52 (d, J = 1.6 Hz, 3H), 1.38–1.29 (m, 6H). ¹³C NMR (125 MHz, CDCl₃, 298 K): δ = 167.54, 167.33, 162.20, 157.25, 154.42, 152.33, 151.35, 151.02, 150.99, 149.92, 149.79, 149.46, 149.08, 148.89, 147.50, 144.86, 143.61, 143.48, 139.48, 138.37, 138.32, 135.76, 131.86, 131.66, 131.61, 130.88, 130.76, 130.06, 129.68, 129.56, 128.06, 127.75, 127.52, 126.19, 124.79, 124.69, 124.29, 123.91, 123.78, 122.95, 122.82, 122.75, 121.49, 119.94, 119.64, 119.54, 119.07, 116.96, 112.84, 107.17, 98.84, 98.82, 51.89, 51.88, 29.62, 25.43, 21.50, 20.77. MALDI-TOF MS: *m/z* = 1040.9835. Elemental analyses calcd (%) for C₅₆H₄₄F₆IrN₆O₃P: C 56.70, H 3.74, N 7.09. Found: C 56.93, H 3.89, N 6.91.

Complex 2. The procedure was similar to that described for the synthesis of complex 1 except [(dOMeppy)₂Ir(μ-Cl)]₂ (301 mg, 0.23 mmol) was used in place of [(ppy)₂Ir(μ-Cl)]₂. Yield: 324 mg, 54%. ¹H NMR (500 MHz, CDCl₃, 298 K, relative to Me₄Si): δ = 9.12 (s,

1H), 8.59 (d, J = 8.5 Hz, 2H), 8.40 (d, J = 19.2 Hz, 2H), 8.21 (d, J = 5.7 Hz, 1H), 8.12 (d, J = 5.4 Hz, 1H), 7.85 (d, J = 5.6 Hz, 1H), 7.81 (d, J = 8.8 Hz, 1H), 7.68 (dd, J = 18.3, 9.1 Hz, 4H), 7.54 (t, J = 5.1 Hz, 2H), 7.38 (d, J = 8.5 Hz, 1H), 7.30 (d, J = 5.6 Hz, 1H), 7.21 (d, J = 7.5 Hz, 1H), 7.09 (d, J = 7.3 Hz, 1H), 7.02 (d, J = 8.8 Hz, 1H), 6.91 (dd, J = 14.2, 6.7 Hz, 3H), 6.58 (d, J = 7.7 Hz, 1H), 6.19 (s, 2H), 5.43 (dd, J = 16.5, 1.9 Hz, 2H), 3.96 (s, 6H), 3.53 (t, J = 14.2 Hz, 6H), 2.76 (s, 3H), 2.64 (s, 3H), 1.35 (d, J = 2.7 Hz, 6H). ¹³C NMR (125 MHz, CDCl₃, 298 K): δ = 166.72, 166.57, 162.26, 162.00, 161.89, 160.20, 160.14, 157.15, 155.01, 154.90, 154.26, 152.24, 151.34, 150.94, 149.85, 149.46, 148.38, 148.32, 147.53, 144.85, 139.38, 137.85, 137.80, 135.81, 131.62, 130.11, 129.83, 129.58, 128.04, 127.71, 127.60, 126.10, 124.63, 124.52, 124.13, 123.43, 123.38, 122.97, 121.50, 121.39, 121.33, 119.92, 119.06, 116.95, 112.82, 108.36, 108.25, 107.16, 98.82, 93.18, 93.11, 55.12, 54.77, 51.88, 29.64, 25.43, 21.55, 20.77. MALDI-TOF MS: *m/z* = 1160.5867. Elemental analyses calcd (%) for C₆₀H₅₂F₆IrN₆O₃P: C 55.17, H 4.01, N 6.43. Found: C 55.58, H 4.27, N 6.09.

Complex 3. The procedure was similar to that described for the synthesis of complex 1 except [(pba)₂Ir(μ-Cl)]₂ (272 mg, 0.23 mmol) was used in place of [(ppy)₂Ir(μ-Cl)]₂ and dichloromethane/ethyl acetate (10:1 v/v) was used as eluent in the column chromatography. Yield: 262 mg, 46%. ¹H NMR (500 MHz, CDCl₃, 298 K, relative to Me₄Si): δ = 9.75 (d, J = 4.8 Hz, 2H), 9.18 (s, 1H), 8.48 (s, 1H), 8.37 (s, 1H), 8.16–8.11 (m, 2H), 8.10–8.05 (m, 2H), 7.89 (ddd, J = 11.0, 10.0, 5.0 Hz, 4H), 7.78 (dd, J = 9.6, 4.6 Hz, 3H), 7.74 (d, J = 5.6 Hz, 1H), 7.71–7.65 (m, 2H), 7.58 (t, J = 7.3 Hz, 2H), 7.38–7.27 (m, 4H), 7.22 (t, J = 7.4 Hz, 1H), 7.09 (d, J = 7.1 Hz, 1H), 7.02 (d, J = 8.8 Hz, 1H), 6.90 (t, J = 7.5 Hz, 1H), 6.74 (d, J = 17.0 Hz, 2H), 6.58 (d, J = 7.7 Hz, 1H), 2.75 (s, 3H), 2.64 (s, 3H), 1.35 (d, J = 2.9 Hz, 6H). ¹³C NMR (125 MHz, CDCl₃, 298 K): δ = 192.60, 165.74, 165.51, 161.99, 157.23, 154.38, 152.99, 151.29, 151.06, 149.74, 149.62, 149.56, 149.41, 149.23, 147.48, 144.91, 140.03, 139.14, 139.08, 137.00, 136.92, 135.74, 132.85, 132.55, 131.61, 130.07, 129.80, 129.73, 128.07, 127.99, 127.54, 126.62, 125.72, 125.61, 125.11, 125.02, 124.81, 124.71, 122.96, 121.50, 121.29, 121.21, 119.97, 118.97, 117.05, 112.85, 107.19, 98.83, 51.88, 31.60, 29.62, 25.41, 22.67, 21.55, 20.76, 14.14. MALDI-TOF MS: *m/z* = 1096.6238. Elemental analyses calcd (%) for C₅₈H₄₄F₆IrN₆O₃P: C 56.08, H 3.57, N 6.77. Found: C 56.36, H 3.68, N 6.53.

Complex 4. The procedure was similar to that described for the synthesis of complex 1 except [(dCF₃ ppy)₂Ir(μ-Cl)]₂ (371 mg, 0.23 mmol) was used in place of [(ppy)₂Ir(μ-Cl)]₂. Yield: 268 mg, 40%. ¹H NMR (500 MHz, CDCl₃, 298 K, relative to Me₄Si): δ = 9.24 (s, 1H), 8.54 (s, 1H), 8.49–8.44 (m, 2H), 8.37 (d, J = 2.2 Hz, 1H), 8.19 (dd, J = 5.6, 1.4 Hz, 1H), 7.97 (dd, J = 10.0, 4.4 Hz, 3H), 7.91 (d, J = 5.8 Hz, 1H), 7.86 (d, J = 5.6 Hz, 1H), 7.75–7.68 (m, 4H), 7.65 (d, J = 8.9 Hz, 1H), 7.59 (d, J = 4.6 Hz, 1H), 7.42 (t, J = 6.3 Hz, 1H), 7.38–7.35 (m, 1H), 7.34–7.28 (m, 2H), 7.22 (t, J = 7.6 Hz, 1H), 7.09 (d, J = 7.1 Hz, 1H), 7.02 (d, J = 8.9 Hz, 1H), 6.90 (t, J = 7.4 Hz, 1H), 6.58 (d, J = 7.7 Hz, 1H), 6.47 (d, J = 17.1 Hz, 2H), 2.76 (d, J = 4.0 Hz, 3H), 2.64 (d, J = 1.6 Hz, 3H), 1.35 (d, J = 3.7 Hz, 6H). ¹³C NMR (125 MHz, CDCl₃, 298 K): δ = 163.06, 162.77, 161.80, 157.06, 154.23, 153.68, 153.29, 153.09, 151.11, 151.01, 150.57, 150.50, 150.18, 149.36, 148.88, 147.50, 144.91, 144.45, 140.71, 139.39, 135.74, 131.59, 131.21, 130.97, 130.79, 129.97, 129.85, 129.57, 128.34, 128.20, 128.07, 127.96, 127.83, 127.52, 126.75, 126.46, 125.59, 124.50, 123.83, 122.95, 122.34, 121.65, 121.50, 119.97, 118.95, 117.09, 112.83, 107.18, 98.89, 98.82, 53.80, 51.92, 51.88, 29.71, 29.62, 29.28, 25.43, 25.39, 21.61, 20.75. MALDI-TOF MS: *m/z* = 1312.3337. Elemental analyses calcd (%) for C₆₀H₄₀F₁₈IrN₆O₃P: C 49.42, H 2.76, N 5.76. Found: C 49.57, H 3.06, N 5.51.

Physical Measurements and Instrumentation. ¹H NMR and ¹³C{¹H} NMR spectra were obtained on a Bruker DRX 500 (500 MHz) spectrometer at 298 K with chemical shifts reported relative to tetramethylsilane (Me₄Si). All MALDI-TOF mass spectra were recorded on a Autoflex speed TOF/TOF mass spectrometer. Elemental analysis was carried out on a Vario micro cube analyzer from Elementar. The single-crystal structure was obtained on a R-AXIS RAPID X-ray single crystal diffractometer.

UV–vis absorption spectra were recorded using a Varian Cary 50 UV–vis spectrophotometer. Steady-state excitation and emission spectra at room temperature and at 77 K were obtained on an Edinburgh Instruments FS5 spectrofluorometer. Measurements of the glass state in ethano/methanol (4:1 v/v) at 77 K were similarly conducted with liquid nitrogen filled in the optical Dewar flask. All of the solutions for the photophysical studies were degassed on a high-vacuum line in a two-compartment cell consisting of a 10 mL Pyrex bulb and a 1 cm path length quartz cuvette that was sealed from the atmosphere by a Bibby Rotaflo HP6 Teflon stopper. The solutions were rigorously degassed with at least four successive freeze–pump–thaw cycles. Luminescence quantum yields were measured by the optical dilute method and a degassed solution of $[\text{Ru}(\text{bpy})_3]\text{Cl}_2$ in acetonitrile ($\phi = 0.062$, excitation wavelength at 436 nm) was used as the reference. Emission lifetime of solution samples were measured on Edinburgh Instrument FLS 920 spectrometer. The excitation source is Edinburgh Instrument picosecond-pulsed diode laser (Model EPL-405) with 405 nm output. The emission decay signals were captured by a Hamamatsu R928 PMT which was connected to a board (Becker and Hickel SPC-130) and analyzed using the exponential fit (tail-fit data analysis) with the model $I(t) = I_0 \exp(-t/\tau)$, where $I(t)$ and I_0 stand for the luminescence intensities at times t and 0.

The thermal bleaching reaction of spirooxazines is known to follow first-order kinetics at various temperatures. The kinetics for the bleaching reaction were determined by measurement of the UV–vis spectral changes at various temperatures by use of a Varian Cary 50 UV–vis spectrophotometer, with temperature controlled by a Lauda RM6 compact low-temperature thermostat. The first-order rate constants were obtained by taking the negative value of the slope of a linear least-squares fit of $\ln[(A - A_\infty)/(A_0 - A_\infty)]$ against time according to eq 1:

$$\ln[(A - A_\infty)/(A_0 - A_\infty)] = -kt \quad (1)$$

where A , A_0 , and A_∞ are the absorbances at the absorption wavelength maximum of the photomerocyanine at times t , 0, and infinity, respectively, and k is the rate constant of the reaction. The kinetics parameters were obtained by a linear least-squares fitting of $\ln(k/T)$ against $1/T$ according to the linear expression of the Eyring equation (eq 2), $\ln k$ against $1/T$ according to the Arrhenius equation (eq 3), and the change in Gibbs free energy of activation (ΔG^\ddagger) at 298 K were determined according to eq 4:

$$\ln(k/T) = -(\Delta H^\ddagger/R)(1/T) + \ln(k_B h^{-1}) + (\Delta S^\ddagger/R) \quad (2)$$

$$\ln(k) = -E_a/RT + \ln A \quad (3)$$

$$\Delta G^\ddagger = \Delta H^\ddagger - T\Delta S^\ddagger \quad (4)$$

where ΔH^\ddagger and ΔS^\ddagger are the changes in activation enthalpy and entropy, respectively, T is the temperature, and k_B , R , h , and A are Boltzmann's constant, the universal gas constant and the Planck constant, and the frequency factor, respectively.

Cyclic voltammetric measurements were performed by using a CH Instruments, Inc. model CHI 660C electrochemical analyzer. Electrochemical measurements were performed in acetonitrile solution with 0.1 M Bu_4NPF_6 as supporting electrolyte at room temperature. The reference electrode was an Ag/AgNO_3 (0.1 mol dm^{-3} in acetonitrile) electrode, and the working electrode was a glassy carbon electrode (CH Instruments, Inc.) with a platinum wire as the counter electrode. The working electrode surface was first polished with a 1 μm alumina slurry. It was then rinsed with ultrapure deionized water and sonicated in a beaker containing ultrapure water for 5 min. The polishing and sonication steps were repeated twice, and the working electrode was finally rinsed under a stream of ultrapure deionized water. The ferrocenium-ferrocene couple ($\text{FcP}_2^{+/0}$) was used as the internal reference.⁶³ All solutions for electrochemical studies were deaerated with prepurified argon gas before measurement.

Computational Methodology. All calculations in this study were performed with the Gaussian 09 program suite.⁶⁸ The ground-state (S_0) geometries of complexes 1–4 were fully optimized in

dichloromethane by density functional theory (DFT) with the hybrid B3LYP functional using the Coulomb-attenuating method (CAM-B3LYP),⁶⁴ in conjunction with the conductor-like polarizable continuum model (CPCM).^{69,70} To compute the singlet–singlet transitions of the four complexes, TDDFT^{71–73} calculations have been performed on the optimized S_0 geometries at the same level of theory. To gain more insight into the emissive states, the geometries of the lowest-lying triplet excited states (T_1) were optimized with the unrestricted formalism, namely, UCAM-B3LYP/CPCM (CH_2Cl_2). Vibrational frequencies of all the stationary points have been computed to verify that each was a minimum (NIMAG = 0) on the potential energy surface. The Cartesian coordinates of the optimized S_0 and T_1 geometries of 1–4 are given in the Supporting Information. For all calculations, the LanL2DZ basis set with effective core potential (ECP)^{74–76} was applied to describe Ir with f -type polarization functions ($\zeta = 0.938$),⁷⁷ whereas the 6-31G(d,p) basis set^{78–80} was utilized to describe all other atoms. All the DFT and TDDFT calculations were performed with a pruned (99,590) grid for numerical integration.

■ ASSOCIATED CONTENT

Supporting Information

The Supporting Information is available free of charge on the ACS Publications website at DOI: 10.1021/acs.organomet.9b00359.

UV–vis absorption spectra of complexes 1–4 in dichloromethane at room temperature; normalized emission spectra of close form and open form complexes 1–4 in EtOH/MeOH (4:1 v/v) at 77 K; data of bleaching reaction kinetics; NMR spectra of the iridium(III) complexes; ground-state geometries of 1–4 optimized in dichloromethane; simulated absorption spectra of 1–4 with first 15 singlet–singlet transitions computed by the TDDFT/CPCM (CH_2Cl_2) method; selected molecular orbitals involved in the transitions; a text file of all computed molecule (PDF)

Cartesian coordinates in a format for convenient visualization (XYZ)

Accession Codes

CCDC 1909997 contains the supplementary crystallographic data for this paper. These data can be obtained free of charge via www.ccdc.cam.ac.uk/data_request/cif, or by emailing data_request@ccdc.cam.ac.uk, or by contacting The Cambridge Crystallographic Data Centre, 12 Union Road, Cambridge CB2 1EZ, UK; fax: +44 1223 336033.

■ AUTHOR INFORMATION

Corresponding Authors

*E-mail: wyyam@hku.hk (V.W.-W.Y.).

*E-mail: wulx@jlu.edu.cn (L.W.).

ORCID

Lixin Wu: 0000-0002-4735-8558

Vivian Wing-Wah Yam: 0000-0001-8349-4429

Notes

The authors declare no competing financial interest.

■ ACKNOWLEDGMENTS

V.W.-W.Y. acknowledges support from The University of Hong Kong under the URC Strategically Oriented Research Theme (SORT) on Functional Materials for Molecular Electronics and Jilin University. This work has been supported by the State Key Laboratory of Supramolecular Structure and Materials of Jilin University and the University Grants

Committee Areas of Excellence Scheme (AoE/P-03/08) and a General Research Fund (GRF) grant from the Research Grants Council of Hong Kong Special Administrative Region, P.R. China (HKU 17334216). The computations were performed using research computing facilities offered by Information Technology Services, The University of Hong Kong.

REFERENCES

- (1) Berkovic, G.; Krongauz, V.; Weiss, V. Spiroprans and Spirooxazines for Memories and Switches. *Chem. Rev.* **2000**, *100*, 1741–1753.
- (2) Kawata, S.; Kawata, Y. Three-Dimensional Optical Data Storage Using Photochromic Materials. *Chem. Rev.* **2000**, *100*, 1777–1788.
- (3) Tian, H.; Yang, S. Recent Progresses on Diarylethene Based Photochromic Switches. *Chem. Soc. Rev.* **2004**, *33*, 85–97.
- (4) Raymo, F. M.; Tomasulo, M. Electron and Energy Transfer Modulation with Photochromic Switches. *Chem. Soc. Rev.* **2005**, *34*, 327–336.
- (5) Tian, H.; Wang, S. Photochromic Bisthiethylene as Multi-Function Switches. *Chem. Commun.* **2007**, *8*, 781–792.
- (6) Jukes, R. T. F.; Bozic, B.; Belsler, P.; De Cola, L.; Hartl, F. Photophysical and Redox Properties of Dinuclear Ru and Os Polypyridyl Complexes with Incorporated Photostable Spiropyran Bridge. *Inorg. Chem.* **2009**, *48*, 1711–1721.
- (7) Poon, C. T.; Lam, W. H.; Wong, H. L.; Yam, V. W. W. A Versatile Photochromic Dithienylethene-Containing A-Diketonate Ligand: Near-Infrared Photochromic Behavior and Photoswitchable Luminescence Properties upon Incorporation of a Boron(III) Center. *J. Am. Chem. Soc.* **2010**, *132*, 13992–13993.
- (8) Yoon, J.; de Silva, A. P. Sterically Hindered Diaryl Benzobis(thiadiazole)s as Effective Photochromic Switches. *Angew. Chem., Int. Ed.* **2015**, *54*, 9754–9756.
- (9) Nakashima, T.; Tsuchie, K.; Kanazawa, R.; Li, R.; Iijima, S.; Galangau, O.; Nakagawa, H.; Mutoh, K.; Kobayashi, Y.; Abe, J.; Kawai, T. Self-Contained Photoacid Generator Triggered by Photocyclization of Triangle Terarylene Backbone. *J. Am. Chem. Soc.* **2015**, *137*, 7023–7026.
- (10) Chu, N. Y. C. Photochromism of spiroindolinaphthoxazine. I. Photophysical Properties. *Can. J. Chem.* **1983**, *61*, 300–305.
- (11) Baillet, G.; Giusti, G.; Guglielmetti, R. Comparative Photodegradation Study between Spiro[indoline—oxazine] and Spiro[indoline—pyran] Derivatives in Solution. *J. Photochem. Photobiol., A* **1993**, *70*, 157–161.
- (12) Khairutdinov, R. F.; Giertz, K.; Hurst, J. K.; Voloshina, E. N.; Voloshin, N. A.; Minkin, V. I. Photochromism of Spirooxazines in Homogeneous Solution and Phospholipid Liposomes. *J. Am. Chem. Soc.* **1998**, *120*, 12707–12713.
- (13) Yam, V. W. W.; Ko, C. C.; Wu, L.; Wong, K. M. C.; Cheung, K. K. Syntheses, Crystal Structure, and Photochromic Properties of Rhenium(I) Complexes Containing the Spironaphthoxazine Moiety. *Organometallics* **2000**, *19*, 1820–1822.
- (14) Bahr, J. L.; Kodis, G.; de la Garza, L.; Lin, S.; Moore, A. L.; Moore, T. A.; Gust, D. Photoswitched Singlet Energy Transfer in a Porphyrin-Spiropyran Dyad. *J. Am. Chem. Soc.* **2001**, *123*, 7124–7133.
- (15) Querol, M.; Bozic, B.; Salluce, N.; Belsler, P. Synthesis, Metal Complex Formation, and Switching Properties of Spiroprans Linked to Chelating Sites. *Polyhedron* **2003**, *22*, 655–664.
- (16) Kopelman, R. A.; Snyder, S. M.; Frank, N. L. Tunable Photochromism of Spirooxazines via Metal Coordination. *J. Am. Chem. Soc.* **2003**, *125*, 13684–13685.
- (17) Ko, C. C.; Wu, L.; Wong, K. M. C.; Zhu, N.; Yam, V. W. W. Synthesis, Characterization and Photochromic Studies of Spirooxazine Containing 2,2'-Bipyridine Ligands and Their Rhenium(I) Tricarbonyl Complexes. *Chem. - Eur. J.* **2004**, *10*, 766–776.
- (18) Jukes, R. T. F.; Bozic, B.; Hartl, F.; Belsler, P.; De Cola, L. Synthesis, Photophysical, Photochemical, and Redox Properties of Nitrospiropyran Substituted with Ru or Os Tris(bipyridine) Complexes. *Inorg. Chem.* **2006**, *45*, 8326–8341.
- (19) Bao, Z.; Ng, K. Y.; Yam, V. W. W.; Ko, C. C.; Zhu, N.; Wu, L. Syntheses, Characterization, and Photochromic Studies of Spirooxazine-Containing 2,2'-Bipyridine Ligands and Their Zinc(II) Thiolate Complexes. *Inorg. Chem.* **2008**, *47*, 8912–8920.
- (20) Ko, C. C.; Wing-Wah Yam, V. Transition Metal Complexes with Photochromic Ligands—Photosensitization and Photoswitchable Properties. *J. Mater. Chem.* **2010**, *20*, 2063–2070.
- (21) Li, Y.; Tam, A. Y. Y.; Wong, K. M. C.; Li, W.; Wu, L.; Yam, V. W. W. Synthesis, Characterization, and the Photochromic, Luminescence, Metallogelation and Liquid-Crystalline Properties of Multifunctional Platinum(II) Bipyridine Complexes. *Chem. - Eur. J.* **2011**, *17*, 8048–8059.
- (22) Liu, Y.; Sun, X.; Wang, Y.; Wu, Z. Quantum Chemical Characterization and Design of Homoleptic Ir(III) Complexes Employing Triphenylamine-Featured Thiazole-Based Ligand for Efficient Phosphors in OLEDs. *Synth. Met.* **2014**, *198*, 67–75.
- (23) Liao, J.; Chi, Y.; Sie, Z. T.; Ku, C. H.; Chang, C. H.; Fox, M. A.; Low, P. J.; Tseng, M. R.; Lee, G. H. Ir(III)-Based Phosphors with Bipyrazolate Ancillaries; Rational Design, Photophysics, and Applications in Organic Light-Emitting Diodes. *Inorg. Chem.* **2015**, *54*, 10811–10821.
- (24) Yang, X.; Feng, Z.; Zhao, J.; Dang, J.; Liu, B.; Zhang, K.; Zhou, G. Pyrimidine-Based Mononuclear and Dinuclear Iridium(III) Complexes for High Performance Organic Light-Emitting Diodes. *ACS Appl. Mater. Interfaces* **2016**, *8*, 33874–33887.
- (25) Chen, Z.; Wang, L.; Su, S.; Zheng, X.; Zhu, N.; Ho, C. L.; Chen, S.; Wong, W. Y. Cyclometalated Iridium(III) Carbene Phosphors for Highly Efficient Blue Organic Light-Emitting Diodes. *ACS Appl. Mater. Interfaces* **2017**, *9*, 40497–40502.
- (26) Kumar, S.; Surati, K. R.; Lawrence, R.; Vamja, A. C.; Yakunin, S.; Kovalenko, M. V.; Santos, E. J. G.; Shih, C. J. Design and Synthesis of Heteroleptic Iridium(III) Phosphors for Efficient Organic Light-Emitting Devices. *Inorg. Chem.* **2017**, *56*, 15304–15313.
- (27) Su, N.; Shen, C.; Zheng, Y. Efficient Electroluminescence of Sky-Blue Iridium(III) Complexes for Organic Light-Emitting Diodes. *Dyes Pigm.* **2018**, *159*, 100–106.
- (28) Xia, J.; Liang, X.; Yan, Z.; Wu, Z.; Zhao, Y.; Zheng, Y.; Zhang, W. Iridium(III) Phosphors with Bis(Diphenylphosphorothioyl)-Amide Ligand for Efficient Green and Sky-Blue OLEDs with EQE of Nearly 28%. *J. Mater. Chem. C* **2018**, *6*, 9010–9016.
- (29) Jang, J. H.; Park, H. J.; Park, J. Y.; Kim, H. U.; Hwang, D. H. Orange Phosphorescent Ir(III) Complexes Consisting of Substituted 2-Phenylbenzothiazole for Solution-Processed Organic Light-Emitting Diodes. *Org. Electron.* **2018**, *60*, 31–37.
- (30) Nonoyama, M. Benzo[h]quinolin-10-yl-N Iridium(III) Complexes. *Bull. Chem. Soc. Jpn.* **1974**, *47*, 767–768.
- (31) Lo, K. K. W.; Chung, C. K.; Lee, T. K. M.; Lui, L. H.; Tsang, K. H. K.; Zhu, N. New Luminescent Cyclometalated Iridium(III) Diimine Complexes as Biological Labeling Reagents. *Inorg. Chem.* **2003**, *42*, 6886–6897.
- (32) Lo, K. K. W.; Chung, C. K.; Zhu, N. Synthesis, Photophysical and Electrochemical Properties, and Biological Labeling Studies of Cyclometalated Iridium(III) Bis(pyridylbenzaldehyde) Complexes: Novel Luminescent Cross-Linkers for Biomolecules. *Chem. - Eur. J.* **2003**, *9*, 475–483.
- (33) Neve, F.; La Deda, M.; Crispini, A.; Bellusci, A.; Puntoriero, F.; Campagna, S. Cationic Cyclometalated Iridium Luminescent Phosphors: Photophysical, Redox, and Structural Characterization. *Organometallics* **2004**, *23*, 5856–5863.
- (34) Smith, R. A.; Stokes, E. C.; Langdon-Jones, E. E.; Platts, J. A.; Kariuki, B. M.; Hallett, A. J.; Pope, S. J. A. Cyclometalated Cinchophen Ligands on Iridium(III): Towards Water-Soluble Complexes with Visible Luminescence. *Dalton Trans* **2013**, *42*, 10347–10357.
- (35) Frey, J.; Curchod, B. F. E.; Scopelliti, R.; Tavernelli, I.; Rothlisberger, U.; Nazeeruddin, M. K.; Baranoff, E. Structure–Property Relationships Based on Hammett Constants in Cyclometalated Iridium(III) Complexes: Their Application to the Design of

- a Fluorine-Free Firpic-Like Emitter. *Dalton Trans* **2014**, 43, 5667–5679.
- (36) Boeyens, J. C. A. The Conformation of Six-Membered Rings. *J. Cryst. Mol. Struct.* **1978**, 8, 317–320.
- (37) Millini, R.; Del Piero, G.; Allegrini, P.; Crisci, L.; Malatesta, V. Structure of Photochromic Spirooxazines. I. 1,3,3-Trimethylspiro[indoline-2,3'-[3H]-naphtho[2,1-b][1,4]oxazine]. *Acta Crystallogr., Sect. C: Cryst. Struct. Commun.* **1991**, 47, 2567–2569.
- (38) Crano, J.; Knowles, D.; Kwiatkowski, P.; Flood, T.; Ross, R.; Chiang, L.; Lasch, J.; Chadha, R.; Siuzdak, C. Structure of Three Novel Photochromic Compounds; X-Ray Crystallographic and Theoretical Studies. *Acta Crystallogr., Sect. B: Struct. Sci.* **1994**, 50, 772–779.
- (39) Chamontin, K.; Lokshin, V.; Guglielmetti, R.; Samat, A.; Pepe, G. 4-Methylspiro [4-azahomoadamantane-5, 3'-[3H]naphth[2, 1-b][1, 4]oxazine], a New Photochromic Spirooxazine. *Acta Crystallogr., Sect. C: Cryst. Struct. Commun.* **1998**, 54, 670–672.
- (40) Favaro, G.; Masetti, F.; Mazzucato, U.; Ottavi, G.; Allegrini, P.; Malatesta, V. Photochromism, Thermochromism and Solvatochromism of Some Spiro[Indolinoxazine]-Photomerocyanine Systems: Effects of Structure and Solvent. *J. Chem. Soc., Faraday Trans.* **1994**, 90, 333–338.
- (41) Ma, Y.; Liu, S.; Yang, H.; Wu, Y.; Yang, C.; Liu, X.; Zhao, Q.; Wu, H.; Liang, J.; Li, F.; Huang, W. Water-Soluble Phosphorescent Iridium(III) Complexes As Multicolor Probes for Imaging of Homocysteine and Cysteine in Living Cells. *J. Mater. Chem.* **2011**, 21, 18974–18982.
- (42) Woo, H.; Cho, S.; Han, Y.; Chae, W. S.; Ahn, D. R.; You, Y.; Nam, W. Synthetic Control Over Photoinduced Electron Transfer in Phosphorescence Zinc Sensors. *J. Am. Chem. Soc.* **2013**, 135, 4771–4787.
- (43) Ru, J.; Guan, L.; Tang, X.; Dou, W.; Yao, X.; Chen, W.; Liu, Y.; Zhang, G.; Liu, W.; Meng, Y.; Wang, C. Turn-on Phosphorescent Chemodosimeter for Hg²⁺ Based on a Cyclometalated Ir(III) Complex and Its Application in Time-Resolved Luminescence Assays and Live Cell Imaging. *Inorg. Chem.* **2014**, 53, 11498–11506.
- (44) Skorka, Ł.; Filapek, M.; Zur, L.; Małeck, J. G.; Pisarski, W.; Olejnik, M.; Danikiewicz, W.; Krompiec, S. Highly Phosphorescent Cyclometalated Iridium(III) Complexes for Optoelectronic Applications: Fine Tuning of the Emission Wavelength through Ancillary Ligands. *J. Phys. Chem. C* **2016**, 120, 7284–7294.
- (45) Cho, W.; Sarada, G.; Maheshwaran, A.; Gal, Y.-S.; Nam, Y.; Yong Lee, J.; Jin, S.-H. Solution-Processable Highly Efficient Deep-Red and Orange Organic Light-Emitting Diodes Based on Multi-Functional Ir(III) Complexes. *J. Mater. Chem. C* **2017**, 5, 10029–10038.
- (46) Liu, J.; Yuan, P. S.; Liang, A. H.; Ma, D. G. Synthesis of a Novel Iridium Complex and Its Exhaustive Investigations of Photophysics, Electrochemistry, Luminescent Mechanism and Electroluminescent Performances. *J. Lumin.* **2018**, 203, 83–89.
- (47) Hobbey, J.; Wilkinson, F. Photochromism of Naphthoxazine-Spiro-Indolines by Direct Excitation and Following Sensitisation by Triplet-Energy Donor. *J. Chem. Soc., Faraday Trans.* **1996**, 92, 1323–1330.
- (48) Tian, Z.; Stairs, R. A.; Wyer, M.; Mosey, N.; Dust, J. M.; Kraft, T. M.; Buncel, E. Spirooxazine to Merocyanine Interconversion in the Presence and Absence of Zinc: Approach to a Bistable Photochemical Switch. *J. Phys. Chem. A* **2010**, 114, 11900–11909.
- (49) Stafforst, T.; Hilvert, D. Kinetic Characterization of Spiropyran in Aqueous Media. *Chem. Commun.* **2009**, 287–288.
- (50) Lo, K. K. W.; Ng, D. C. M.; Chung, C. K. First Examples of Luminescent Cyclometalated Iridium(III) Complexes as Labeling Reagents for Biological Substrates. *Organometallics* **2001**, 20, 4999–5001.
- (51) Lo, K. K. W.; Chan, J. S. W.; Lui, L. H.; Chung, C. K. Novel Luminescent Cyclometalated Iridium(III) Diimine Complexes That Contain a Biotin Moiety. *Organometallics* **2004**, 23, 3108–3116.
- (52) Lepeltier, M.; Kwok-Ming Lee, T.; Kam-Wing Lo, K.; Toupet, L.; Le Bozec, H.; Guerchais, V. Synthesis, Structure, and Photo-physical and Electrochemical Properties of Cyclometalated Iridium(III) Complexes with Phenylated Bipyridine Ligands. *Eur. J. Inorg. Chem.* **2005**, 2005, 110–117.
- (53) Hanss, D.; Freys, J. C.; Bernardinelli, G.; Wenger, O. S. Cyclometalated Iridium(III) Complexes as Photosensitizers for Long-Range Electron Transfer: Occurrence of a Coulomb Barrier. *Eur. J. Inorg. Chem.* **2009**, 2009, 4850–4859.
- (54) Chiridon, D. N.; McCusker, C. E.; Castellano, F. N.; Bernhard, S. Tracking of Tuning Effects in Bis-Cyclometalated Iridium Complexes: A Combined Time Resolved Infrared Spectroscopy, Electrochemical, and Computational Study. *Inorg. Chem.* **2013**, 52, 8795–8804.
- (55) Lee, J.; Park, H.; Park, K. M.; Kim, J.; Lee, J. Y.; Kang, Y. Deep-Blue Phosphorescent Iridium(III) Dyes Based on Fluorine functionalized Bis(2,30-Bipyridyl) Ligand for Efficient Organic Light-Emitting Diodes. *Dyes Pigm.* **2015**, 123, 235–241.
- (56) Pritchard, V. E.; Rota Martir, D.; Zysman-Colman, E.; Hardie, M. J. Multimetallic and Mixed Environment Iridium(III) Complexes: A Modular Approach to Luminescence Tuning Using a Host Platform. *Chem. - Eur. J.* **2017**, 23, 8839–8849.
- (57) Ryan, D. M.; Coggins, M. K.; Concepcion, J. J.; Ashford, D. L.; Fang, Z.; Alibabaei, L.; Ma, D.; Meyer, T. J.; Waters, M. L. Synthesis and Electrocatalytic Water Oxidation by Electrode-Bound Helical Peptide Chromophore-Catalyst Assemblies. *Inorg. Chem.* **2014**, 53, 8120–8128.
- (58) Kim, M. R.; Cheong, I. W. Stimuli-Triggered Formation of Polymersomes from W/O/W Multiple Double Emulsion Droplets Containing Poly(styrene)-block-poly (N-isopropylacrylamide-co-spiro-naphthoxazine methacryloyl). *Langmuir* **2016**, 32, 9223–9228.
- (59) Xu, Q. L.; Wang, C. C.; Li, T. Y.; Teng, M. Y.; Zhang, S.; Jing, Y. M.; Yang, X.; Li, W. N.; Lin, C.; Zheng, Y. X.; Zuo, J. L.; You, X. Z. Syntheses, Photoluminescence, and Electroluminescence of a Series of Iridium Complexes with Trifluoromethyl-Substituted 2-Phenylpyridine as the Main Ligands and Tetraphenylimidodiphosphate as the Ancillary Ligand. *Inorg. Chem.* **2013**, 52, 4916–4925.
- (60) Astles, P. C.; Brealey, C.; Brown, T. J.; Facchini, V.; Handscombe, C.; Harris, N. V.; McCarthy, C.; McLay, I. M.; Porter, B.; Roach, A. G.; Sargent, C.; Smith, C.; Walsh, R. J. A. Selective Endothelin A Receptor Antagonists. 3. Discovery and Structure-Activity Relationships of a Series of 4-Phenoxybutanoic Acid Derivatives. *J. Med. Chem.* **1998**, 41, 2732–2744.
- (61) Lu, F.; Nabeshima, T. A Highly Selective And Sensitive Turn-On Chemodosimeter for Hypochlorous Acid Based on An Iridium(III) Complex and Its Application to Bioimaging. *Dalton Trans* **2014**, 43, 9529–9536.
- (62) Paul, A.; Das, N.; Halpin, Y.; Vos, J. G.; Pryce, M. T. Carboxy Derivatized Ir(III) Complexes: Synthesis, Electrochemistry, Photo-physical Properties and Photocatalytic Hydrogen Generation. *Dalton Trans* **2015**, 44, 10423–10430.
- (63) Connelly, N. G.; Geiger, W. E. Chemical Redox Agents for Organometallic Chemistry. *Chem. Rev.* **1996**, 96, 877–910.
- (64) Yanai, T.; Tew, D. P.; Handy, N. C. A New Hybrid Exchange-Correlation Functional Using the Coulomb-Attenuating Method (CAM-B3LYP). *Chem. Phys. Lett.* **2004**, 393, 51–57.
- (65) Jacquemin, D.; Perpète, E. A.; Scalmani, G.; Frisch, M. J.; Kobayashi, R.; Adamo, C. Assessment of the Efficiency of Long-Range Corrected Functionals for Some Properties of Large Compounds. *J. Chem. Phys.* **2007**, 126, 144105.
- (66) Nayyar, I. H.; Masunov, A. E.; Tretiak, S. Comparison of TD-DFT Methods for the Calculation of Two-Photon Absorption Spectra of Oligophenylvinyls. *J. Phys. Chem. C* **2013**, 117, 18170–18189.
- (67) Caricato, M. Towards the Accurate Simulation of UV/Vis Spectra in Solution: Combining the EOM-CCSD Method with Polarizable Solvation Models within State-Specific and Linear-Response Formalisms. *Photochemistry* **2014**, 42, 197–214.
- (68) Frisch, M. J.; Trucks, G. W.; Schlegel, H. B.; Scuseria, G. E.; Robb, M. A.; Cheeseman, J. R.; Scalmani, G.; Barone, V.; Mennucci, B.; Petersson, G. A.; Nakatsuji, H.; Caricato, M.; Li, X.; Hratchian, H. P.; Izmaylov, A. F.; Bloino, J.; Zheng, G.; Sonnenberg, J. L.; Hada, M.;

Ehara, M.; Toyota, K.; Fukuda, R.; Hasegawa, J.; Ishida, M.; Nakajima, T.; Honda, Y.; Kitao, O.; Nakai, H.; Vreven, T.; Montgomery, J. A., Jr.; Peralta, J. E.; Ogliaro, F.; Bearpark, M.; Heyd, J. J.; Brothers, E.; Kudin, K. N.; Staroverov, V. N.; Kobayashi, R.; Normand, J.; Raghavachari, K.; Rendell, A.; Burant, J. C.; Iyengar, S. S.; Tomasi, J.; Cossi, M.; Rega, N.; Millam, J. M.; Klene, M.; Knox, J. E.; Cross, J. B.; Bakken, V.; Adamo, C.; Jaramillo, J.; Gomperts, R.; Stratmann, R. E.; Yazyev, O.; Austin, A. J.; Cammi, R.; Pomelli, C.; Ochterski, J. W.; Martin, R. L.; Morokuma, K.; Zakrzewski, V. G.; Voth, G. A.; Salvador, P.; Dannenberg, J. J.; Dapprich, S.; Daniels, A. D.; Farkas, O.; Foresman, J. B.; Ortiz, J. V.; Cioslowski, J.; Fox, D. J. *Gaussian 09*, revision D.01; Gaussian, Inc.: Wallingford, CT, 2009.

(69) Barone, V.; Cossi, M. Quantum Calculation of Molecular Energies and Energy Gradients in Solution by a Conductor Solvent Model. *J. Phys. Chem. A* **1998**, *102*, 1995–2001.

(70) Cossi, M.; Rega, N.; Scalmani, G.; Barone, V. Energies, Structures, and Electronic Properties of Molecules in Solution with the C-PCM Solvation Model. *J. Comput. Chem.* **2003**, *24*, 669–681.

(71) Stratmann, R. E.; Scuseria, G. E.; Frisch, M. J. An Efficient Implementation of Time-Dependent Density-Functional Theory for the Calculation of Excitation Energies of Large Molecules. *J. Chem. Phys.* **1998**, *109*, 8218–8224.

(72) Bauernschmitt, R.; Ahlrichs, R. Treatment of Electronic Excitations within the Adiabatic Approximation of Time Dependent Density Functional Theory. *Chem. Phys. Lett.* **1996**, *256*, 454–464.

(73) Casida, M. E.; Jamorski, C.; Casida, K. C.; Salahub, D. R. Molecular Excitation Energies to High-Lying Bound States from Time-dependent Density-Functional Response Theory: Characterization and Correction of the Time-Dependent Local Density Approximation Ionization Threshold. *J. Chem. Phys.* **1998**, *108*, 4439–4449.

(74) Hay, P. J.; Wadt, W. R. Ab Initio Effective Core Potentials for Molecular Calculations. Potentials for K to Au Including the Outermost Core Orbitals. *J. Chem. Phys.* **1985**, *82*, 270–283.

(75) Wadt, W. R.; Hay, P. J. Ab Initio Effective Core Potentials for Molecular Calculations. Potentials for Main Group Elements Na to Bi. *J. Chem. Phys.* **1985**, *82*, 284–298.

(76) Hay, P. J.; Wadt, W. R. Ab Initio Effective Core Potentials for Molecular Calculations. Potentials for K to Au Including the Outermost Core Orbitals. *J. Chem. Phys.* **1985**, *82*, 299–310.

(77) Ehlers, A. W.; Böhme, M.; Dapprich, S.; Gobbi, A.; Höllwarth, A.; Jonas, V.; Köhler, K. F.; Stegmann, R.; Veldkamp, A.; Frenking, G. A Set of *f*-Polarization Functions for Pseudo-Potential Basis Sets of the Transition Metals Sc–Cu, Y–Ag and La–Au. *Chem. Phys. Lett.* **1993**, *208*, 111–114.

(78) Hehre, W. J.; Ditchfield, R.; Pople, J. A. Self-Consistent Molecular Orbital Methods. XII. Further Extensions of Gaussian-Type Basis Sets for Sse in Molecular Orbital Studies of Organic Molecules. *J. Chem. Phys.* **1972**, *56*, 2257–2261.

(79) Hariharan, P. C.; Pople, J. A. The Influence of Polarization Functions on Molecular Orbital Hydrogenation Energies. *Theor. Chim. Acta.* **1973**, *28*, 213–222.

(80) Francl, M. M.; Pietro, W. J.; Hehre, W. J.; Binkley, J. S.; Gordon, M. S.; Defrees, D. J.; Pople, J. A. Self-Consistent Molecular Orbital Methods. XXIII. A Polarization-Type Basis Set for Second-Row Elements. *J. Chem. Phys.* **1982**, *77*, 3654–3665.